Modeling the phase-change processes in pulsed laser-irradiated InSb

R. Černý
Department of Physics, Faculty of Civil Engineering, Czech Technical University, Thákurova 7, 166 29 Prague 6, Czech Republic

V. Cháb
Institute of Physics of the Academy of Sciences of the Czech Republic, Cukrovarnická 10, 160 00 Prague 6, Czech Republic

G. Ivlev and E. Gatskevich
Institute of Electronics of the Belarus Academy of Sciences, 22 Logoiskii Trakt, 220090 Minsk, Belarus

P. Přikryl
Mathematical Institute of the Academy of Sciences of the Czech Republic, Žitná 25, 115 67 Prague 1, Czech Republic
(Received 2 November 1998)

Both theoretical and experimental analyses of pulsed laser-induced phase-change processes in the near-surface region of monocrystalline bulk InSb are treated in the paper. In the theoretical part, thermal equilibrium and nonequilibrium models of melting, recrystallization, and evaporation are formulated to describe transport phenomena in the material induced by laser irradiation. In the experimental part, (110) and (111) InSb samples irradiated by ruby [694 nm, 80 ns full width at half maximum (FWHM)], and ArF (193 nm, 10 ns FWHM) lasers were studied. Time-resolved reflectivity measurements were performed in order to determine the melting thresholds and surface-melt durations. Auger electron spectroscopy and low-energy electron diffraction methods were employed to monitor surface modifications. A combination of experimental measurements and computer simulations reveals that, while for ruby laser the material remains crystalline after irradiation, for ArF laser the InSb sample is amorphized; the amorphization threshold is estimated to be $\sim 4-5$ m/s. The decomposition of InSb at temperatures close to its melting point was also observed, the decomposition temperature being estimated within the range 900–950 K. [S0163-1829(99)09915-4]

I. INTRODUCTION

Laser irradiation of semiconductors has been widely used in connection with solid-phase epitaxy (following doping with ion implantation) as an alternative technique to the conventional thermal heating, restoring the implanted region to a single-crystal state.[1] The process of pulsed-laser annealing of semiconductor surfaces provides a way of rapid adiabatic melting, followed by liquid-phase epitaxial regrowth. The heating and cooling rates achieved in this way have higher orders of magnitude, compared to more conventional methods. Furthermore, the results of many previous experiments[2] show that laser annealing can be used to produce atomically clean surfaces with altered electronic and structural properties. Silicon surfaces under pulsed laser irradiation have been extensively studied using different surface sensitive techniques, such as low-energy electron diffraction (LEED),[3] Auger electron spectroscopy (AES),[4] ultraviolet photoemission spectroscopy,[5] scanning tunneling microscopy,[6] and inverse photoemission.[7] It was found by these methods that laser annealing can produce geometric surface structures, which cannot be obtained by any annealing procedure. A well-known example is the occurrence of a (1×1) LEED pattern on the Si(111) and Si(100) surfaces.[6,8,9] The detailed structure is still unclear, but most of the data are consistent with a model showing an absence of long-range order on these (1×1) laser-annealed surfaces.

To illustrate the application of laser annealing on crystal faces of compound semiconductors, especially those in which one of the components is volatile, the results obtained from the low-index faces of GaAs can be used. The LEED pattern obtained for the (100), (110), and (111) orientations following irradiation at an energy density just above the melting threshold was of basically low-quality (1×1), suggesting no long-range ordered reconstruction, as is normally observed after conventional thermal annealing. These observations are consistent with AES and Rutherford backscattering spectroscopy results, which indicate the existence of excess Ga in some parts of an irradiated surface, and which are nonstoichiometric in the near-surface region. In accordance with these very early studies of laser-pulse interaction with III-V semiconductor surfaces,[10] the alteration of the surface stoichiometry has also been observed in the most recent studies. The resulting crystallographic quality of the processed surface was poor. However, it has been demonstrated by low-power pulsed-laser annealing that, in cases where the temperature is kept strictly below a certain critical value at any point within the irradiated area, the compound semiconductors can be processed without decomposition of the surface.[2]

Recently, helium-atom scattering experiments have been reported,[11] showing InSb as a III-V candidate in order to study laser-induced phase transformations (with the value of the decomposition temperature being close to melting point). Ion bombardment experiments indicated that the sputtering proceeded layer-by-layer, with no preferential removal of any element. Time-resolved reflectivity (TRR) measurements on a related material GaSb (Ref. 12) have illustrated

the formation of two metastable liquid phases through the application of nanosecond laser pulses. This fact attracted our attention to this type of III-V compounds, and lead us to study the nonequilibrium phase diagrams.

Most theoretical studies of laser-induced melting, solidification, and ablation have been based on various phenomenological models dealing with one-component materials.[13] Pioneering work on the crystallization of amorphous silicon has extended these kind of models to situations where the presence of two or more different phases exists. Lately, it has been applied to outline the segregation processes in two-component semiconductor alloys.[14]

In the present paper, we will show experimental and numerical data concerning the dynamics of melting and solidification processes in InSb monocrystalline samples, as induced by excimer and ruby-laser pulses. The melting time is simulated by equilibrium and nonequilibrium models developed for a one-component material, which also allows us to implement induced chemical and structural changes to the irradiated area. The resulting structure and stoichiometry are monitored by LEED/AES facilities. A combination of experimental and theoretical data leads to the estimations of the amorphization threshold and the decomposition temperature.

II. MATHEMATICAL MODEL

We will assume that InSb within a certain range of temperatures (i.e., energy densities of the laser) can be considered as a one-component material. Thus, we will employ a relatively simple thermal model, which we developed earlier for elemental semiconductors.[13] We will summarize the main features of the model here, for the convenience of the reader.

The one-dimensional heat conduction in the material sample can be described in a general case, when both solid and liquid phases are present, as follows:

$$\rho c_i \frac{\partial T}{\partial t} = \frac{\partial}{\partial x}\left(K_i \frac{\partial T}{\partial x}\right) + S(x,t), \quad i = l,s, \tag{1}$$

where T is the temperature, ρ the density, c_i the specific heat, K_i the thermal conductivity, and the heat source term $S(x,t)$ can be expressed as

$$S(x,t) = [1 - R(t)]\alpha I_0(t)\exp(-\alpha x),$$

I_0 being the power density of the laser, R the reflectivity, and α the optical absorption coefficient. The indices l,s denote the liquid and solid phase, respectively.

At the moving interface $Z(t)$ between the solid and liquid phases we can write the internal energy balance as

$$\rho L(T_Z)\dot{Z}(t) = K_s \left.\frac{\partial T}{\partial x}\right|_{x=Z^+} - K_l \left.\frac{\partial T}{\partial x}\right|_{x=Z^-}, \tag{2}$$

where $\dot{Z}(t)$ is the velocity of the moving boundary between the solid and liquid phases, and the latent heat of fusion generally depends on temperature as follows:

$$L(T_Z) = L_{eq} + (T_Z - T_{eq})(c_l - c_s),$$

where T_Z is the temperature of the interface.

In solving our Stefan-like problem, an additional condition at the interface has to be formulated. It primarily depends on the choice of the type of the phase change model.

For an equilibrium model (EQ model in what follows) we use the local thermodynamic equilibrium condition in the form

$$T_Z = T_{eq}, \tag{3}$$

where T_{eq} is the equilibrium melting temperature.

For a nonequilibrium model (NEQ model in what follows) we replace (3) by an interface response function,

$$\dot{Z}(T_Z) = -C_1 \exp\left(-\frac{Q}{k_B T_Z}\right)\left\{1 - \exp\left[-\frac{L_p}{k_B}\left(\frac{1}{T_Z} - \frac{1}{T_{eq}}\right)\right]\right\}, \tag{4}$$

where Q denotes the activation energy for self-diffusion in the liquid, L_p is the latent heat of fusion per particle, and C_1 is a material constant. The other boundary and initial conditions are formulated in a common way:

$$\left.\frac{\partial T}{\partial x}\right|_{x=0^+} = 0, \tag{5}$$

$$T(D,t) = T_0, \tag{6}$$

$$T(x,0) = T_0, \tag{7}$$

$$Z(0) = 0, \tag{8}$$

where D is the thickness of the material sample.

As the sample is generally optically nonhomogeneous due to the dependence of the complex refraction index on temperature, we have to calculate the reflectivity using the following formulas (see Ref. 15):

$$R = (R_{\mathrm{TE}} + R_{\mathrm{TM}})/2, \tag{9}$$

where R_{TE} and R_{TM} are the reflectivities of TE and TM waves, respectively,

$$R_i = |\hat{r}_i|^2, \quad i = \mathrm{TE,TM}, \tag{10}$$

$$\hat{r}_{\mathrm{TE}} = \frac{(\hat{m}_{11} + \hat{m}_{12}\hat{P}_3)\hat{P}_1 - (\hat{m}_{21} + \hat{m}_{22}\hat{P}_3)}{(\hat{m}_{11} + \hat{m}_{12}\hat{P}_3)\hat{P}_1 + (\hat{m}_{21} + \hat{m}_{22}\hat{P}_3)}, \tag{11}$$

$$\hat{r}_{\mathrm{TM}} = \frac{(\hat{m}_{11} - \hat{m}_{12}\hat{Q}_3)\hat{Q}_1 - (-\hat{m}_{21} + \hat{m}_{22}\hat{Q}_3)}{(\hat{m}_{11} - \hat{m}_{12}\hat{Q}_3)\hat{Q}_1 + (-\hat{m}_{21} + \hat{m}_{22}\hat{Q}_3)}, \tag{12}$$

$$[M] = \begin{bmatrix} \hat{m}_{11} & \hat{m}_{12} \\ \hat{m}_{21} & \hat{m}_{22} \end{bmatrix} = \prod_{k=1}^{N} [M_k], \tag{13}$$

$$[M_k]=\begin{bmatrix} \cos(k_0\hat{n}\Delta x_k\cos\hat{\theta}_k) & -i\hat{P}_k^{-1}\sin(k_0\hat{n}\Delta x_k\cos\hat{\theta}_k) \\ -i\hat{P}_k\sin(k_0\hat{n}\Delta x_k\cos\hat{\theta}_k) & \cos(k_0\hat{n}\Delta x_k\cos\hat{\theta}_k) \end{bmatrix} \tag{14}$$

for the TE wave, and

$$[M_k]=\begin{bmatrix} \cos(k_0\hat{n}\Delta x_k\cos\hat{\theta}_k) & -i\hat{Q}_k^{-1}\sin(k_0\hat{n}\Delta x_k\cos\hat{\theta}_k) \\ -i\hat{Q}_k\sin(k_0\hat{n}\Delta x_k\cos\hat{\theta}_k) & \cos(k_0\hat{n}\Delta x_k\cos\hat{\theta}_k) \end{bmatrix} \tag{15}$$

for the TM wave, $\hat{P}_j=p\hat{n}_j\cos\hat{\theta}_j$, $\hat{Q}_j=q\cos\hat{\theta}_j/\hat{n}_j$, $p=\sqrt{\epsilon_0/\mu_0}$, $q=1/p$, the indices 1 and 3 of $\hat{P}$, $\hat{Q}$ denote optically homogeneous media within the space intervals $(-\infty,0)$ and $(D,+\infty)$, $\hat{n}$ is the complex refraction index, Δx_k is the thickness of a layer with $\hat{n}_k=$const., in the x direction, k_0 is the wave number, and $\hat{\theta}_j$ is the angle of incidence.

III. EXPERIMENT

InSb samples were prepared by being cleaved in air off a bar, along the (110) plane, or by being cut into a wafer with a mechanically polished (111) surface. The samples were irradiated, either in air or under UHV conditions ($<10^{-10}$ Torr, Omicron LEED/AES facility). An ArF ($\lambda=193$ nm, 10 ns at FWHM, Lambda EMG 100) and a ruby ($\lambda=694$ nm, 80 ns at FWHM) laser were used for sample processing. Typical laser-spot dimensions produced on the surface were $1-2\times2-4$ mm. The energy density of the laser beam was measured with the relative reproducibility between different experiments being about 5%. Absolute calibration was carried out using a standard value for the melting threshold on a Si(100) surface. By focusing the laser spot, energy density E was varied between 10–400 mJ/cm^2 for the ArF excimer laser and between 50–1200 mJ/cm^2 for the ruby laser. Changes in the optical parameters of the surface during pulse incidence were monitored *in situ* by the TRR method, using the HeNe cw laser ($\lambda=633$ nm) (Ref. 16) during processing with the ArF laser and using the Nd:glass laser ($\lambda=1.06$ μm, 0.5 ms) (Ref. 17) for irradiation with the ruby laser.

IV. RESULTS AND DISCUSSION

Figures 1(a) and 1(b) show the comparison of surface-melt durations determined both experimentally using the TRR measurements, and numerically using EQ and NEQ models. The agreement seems to be very good for the ruby laser and very poor for the ArF laser (for both EQ and NEQ models); the differences between the EQ and NEQ models being very small (up to 3.5%). We tried first to find an explanation for this discrepancy using the shape of TRR curves shown in Figs. 2(a) and 2(b). However, the differences observed are apparently due mainly to the different pulse lengths of applied ArF and ruby lasers. It should be mentioned only that the increase in the TRR curves maximum (with increasing energy density just above the melting threshold) is not so pronounced here, as with Si and Ge, even if the change in the reflectivity between the liquid and solid phases is of the same order of magnitude for all the three materials. The origin of this effect has not yet been fully understood, but it could be connected with structural and concentration changes, which were found from the LEED/AES analyses (see further discussion).

The AES spectra of ArF laser irradiated samples do not show any significant changes in the In/Sb intensity ratio (~1) at energy densities below and at the melting threshold (60 mJ/cm^2 on a virgin surface, which was not irradiated before). Figure 3 demonstrates the In/Sb intensity ratio plotted as a function of energy densities higher than the melting threshold. It clearly indicates that the decomposition of InSb begins at approximately 80 mJ/cm^2 and is connected with a

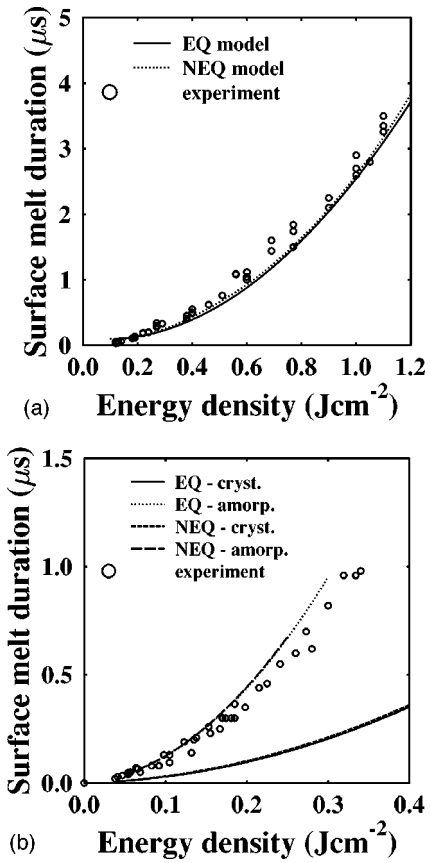

FIG. 1. Surface-melt durations determined experimentally by TRR measurements and theoretically using EQ and NEQ models for (a) ruby laser and (b) ArF laser.

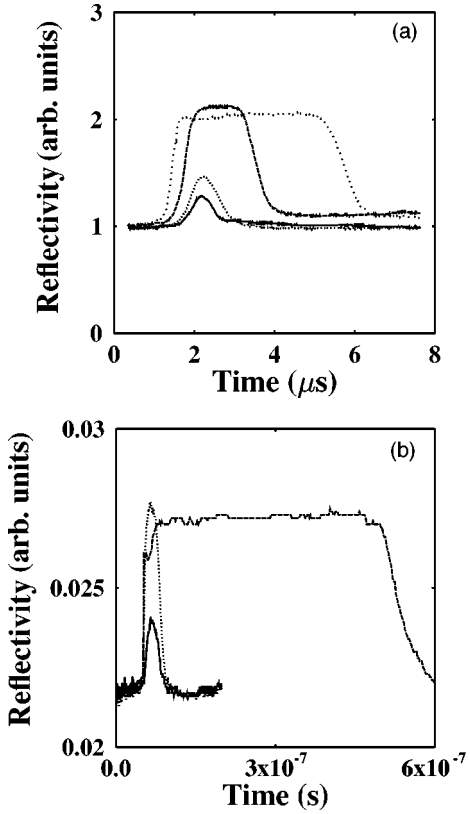

FIG. 2. Examples of measured TRR curves for (a) ruby laser and (b) ArF laser.

depletion in Sb from the topmost surface layers. The loss of antimony has its sharpest peak at approximately 250 mJ/cm^2 (where the atomic ratio of In/Sb is as high as eight). At higher energy densities the In/Sb ratio finally decreases to a constant value of approximately $\sim$2.5. This value is not changed by further irradiation of the layer, with the energy density remaining the same as for the interval of the values used in the experiments. The equilibrium phase diagram does not show any significant feature at this particular concentration of both elements. Thus, the formation of the surface showing this In/Sb ratio can be considered as a product of nonequilibrium solidification of the molten and decomposed InSb layer. The formation of the modified layer is probably due to faster diffusion of In atoms in the melt towards the surface. The question remains if the depleted Sb atoms are evaporated into the vacuum, or if they segregate at liquid/solid interface during the melting and solidification process. The modified layer was further investigated to determine the melting threshold. Measuring the melt duration as a function of applied energy density, we found that an already irradiated surface showed a lower melting threshold of about approximately 20 mJ/cm^2.

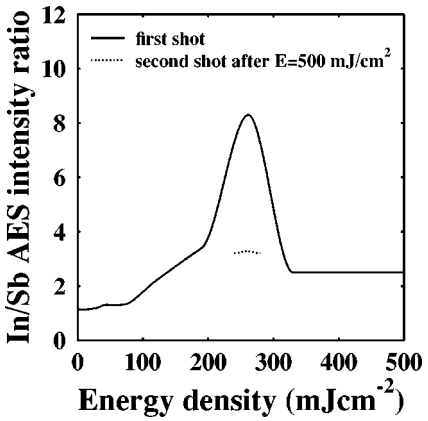

FIG. 3. Summary of AES measurements of ArF laser-irradiated InSb samples.

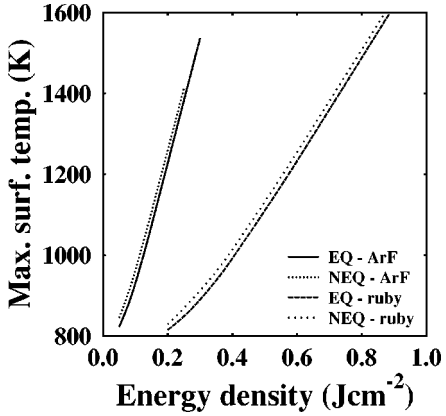

FIG. 4. Maximum surface temperatures of InSb samples calculated using EQ and NEQ models.

Figure 4 shows the surface temperatures, as calculated using both EQ and NEQ models for both types of processing lasers. Apparently, the comparison with the experimental In/Sb ratio obtained with ArF laser irradiation sets the decomposition temperature of InSb somewhere in the range of 900–950 K for both models. The surface temperature for one particular energy density, as calculated using the EQ and NEQ models, differs as high as 30–35 K in the vicinity of the decomposition temperature. This difference could help us to resolve the degree of the deviation from the equilibrium. Nevertheless, this difference is experimentally hard to distinguish, and results obtained by both types of models are in reasonable agreement with the previous experimental findings,[11] which showed that InSb possesses decomposition temperature very close to its equilibrium melting point of 798 K.

To improve the simulation of the experimental TRR spectra for ArF laser irradiation, we considered the changes in the composition of a processed layer, as taken from the AES intensity ratio, and used the temperature of melting given by the equilibrium In-Sb phase diagram. This procedure did not lead to any significant improvement in the agreement between the theory and the experimental data for ArF laser irradiation. The calculated melt duration increased by only a small fraction, giving considerably smaller values in comparison with the experimental ones. We concluded that the InSb decomposition, and its subsequent deviation from the stoichiometry, is not the dominating mechanism determining the melt duration.

A significant progress in the simulation was achieved after analysis of the LEED data taken on the surface during processing with the ArF laser. The LEED pattern corresponds to a (1$\times$1) structure (which is natural on a cleaved 110 face) after irradiation with energy densities below, and at the melting threshold. The further increase in energy densities led both to an increase in the background and the disap-

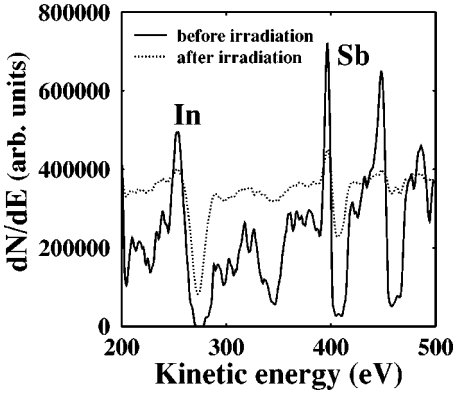

FIG. 5. Example of AES spectra before and after ArF laser irradiation.

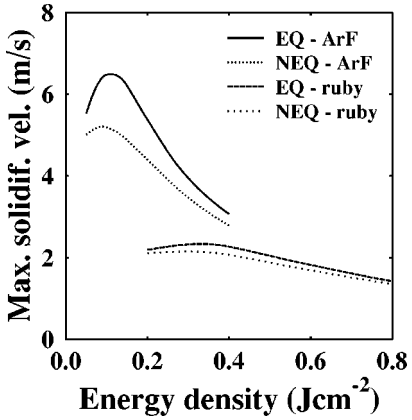

FIG. 6. Maximum solidification velocities calculated using EQ and NEQ models.

pearance of diffraction spots. This can be interpreted as amorphization of the irradiated layer. This interpretation is also supported by analysis of the overall shape of AES spectra. As shown in Fig. 5, the AES spectra, taken after ArF laser irradiation, exhibit smoothing of the structure in In and Sb peaks, as compared to its state before irradiation. This indicates an increasing structural and chemical disorder, as can be expected from an amorphous material. Thus, we included in our mathematical model estimated material data for amorphous InSb, and repeated the mathematical simulation of the melt duration as a function of energy density. The quantity, which considerably differs for amorphous and crystalline phases of different semiconductors, represents the thermal conductivity. The reflectivity in the vacuum ultraviolet region does not change significantly at this phase transition. Furthermore, the generally observed decrease in the melting point does not influence practically (in the case of InSb) the value of the theoretical melt duration, as can be seen from the above calculations. Because the value of thermal conductivity was not available (as far as we know), we used in the simulation the value that was found for other semiconductors, such as Si ($\sim$0.02 W/cmK, see Ref. 18). The model is further simplified—we suppose that the decomposition and amorphization processes do not change the heat balance in the molten layer. This is not included implicitly into the model because the compound is treated as a one-component material, which undergoes the melting and crystallization phase transition. Because the data obtained with the ruby laser were successfully reproduced in this approximation, even if the decomposition temperature was reached, this shows that the process does not significantly contribute to the heat balance. Figure 1(b) demonstrates this effect. Here, we achieved a reasonable agreement with the experimental melt duration for both EQ and NEQ models.

However, the question still remains why, with ruby-laser irradiation, the material crystallizes and the ArF excimer laser pulses amorphize the processed layer. Generally, such a transition between the crystalline and amorphous phases following laser irradiation is related to a threshold in the solidification velocity. If the solidification proceeds with higher velocities, the laser irradiation leads to amorphization of the processed material. Its existence has been demonstrated for a Si(111) surface. There are, in fact, two thresholds. First, the solidification with velocities close to the first threshold produces the disordered top most layer, characterized by a (1×1) LEED pattern instead of (7x7), corresponding to equilibrium surface. The second, having a value of $\sim$15 m/s, is connected with amorphization of the entire layer molten with a single laser pulse. In the case of InSb we observed the absence of a LEED pattern, signalizing a structural disorder (at least in the three or four topmost layers). The Auger peak In/Sb intensity ratio demonstrates the presence of a chemical disorder to an identical depth as found by the LEED information. In Fig. 6 we present the calculated maximum solidification velocities (using both EQ and NEQ models) for irradiation by ruby and ArF lasers. The velocities observed for ArF laser irradiation are apparently significantly higher than those for the ruby laser. Taking into account that the agreement between the experimental and theoretical time of melting for a ruby laser was obtained using a model where InSb is treated as a one component, crystalline material, these results allow us to estimate the value of the velocity, corresponding to an amorphization threshold of $\sim$4–5 m/s. If the process of melting and solidification is a nonequilibrium form of phase transition, the maximum solidification velocities for the ArF laser (given by the NEQ model) differ by a maximum as much as 1.3 m/s less than those resulting from the EQ model.

To summarize the processing of InSb with ArF excimer-laser pulses, irradiation with energy densities below 80 mJ/cm^2 and above the melting threshold produces a surface with an unchanged structure and chemical composition, the dominating mechanism of the solidification is the homoepitaxial growth. Higher-energy densities cause the decomposition of InSb, accompanied by strong chemical and structural disorder during liquid phase. Solidification with velocities higher than $\sim$4–5 m/s preserves the amorphous character of the layer. For ruby-laser processing the decomposition temperature is also reached during liquid phase but the solidification is slow enough to allow recovery of the original state of the irradiated layer. This result refutes to the interpretation of changed In/Sb ratio as a result of Sb evaporation. Instead, it supports the idea of the existence of a gradient of both elements, in the direction going from the surface towards the bulk of the sample.

V. CONCLUSIONS

The results of the theoretical simulation of the experimentally found dependence of the melting time on the energy

density for InSb samples irradiated with ArF excimer and ruby-laser pulses can be outlined as follows: (i) The InSb decomposition temperature T_{dc} is very close to its melting point (798 K), according to the numerical estimate $T_{dc} \in (900\ \mathrm{K}, 950\ \mathrm{K})$. (ii) An amorphization threshold for InSb solidification velocity was estimated to be approximately $v_A \sim 4-5$ m/s. During the amorphization process the stoichiometry of the irradiated layer is changed, forming a stable or metastable alloy, which does not correspond to any significant point of the equilibrium phase diagram. (iii) The simplified, one-component EQ and NEQ models resulted in a reasonable agreement with the experimental data for the ruby laser. With ArF excimer-laser irradiation, the change in the thermal conductivity as a result of layer irradiation has to be supposed in order to fit the experimental values of the melting time. (iv) The significant differences in the NEQ and EQ description of the melting and solidification process were found for maximum surface temperatures close to the melting point, and for maximum solidification velocities.

ACKNOWLEDGMENT

This paper has been supported by the Grant Agency of the Czech Academy of Sciences under Grant No. A1010719.

[1] *Laser-Beam Interaction with Materials,* edited by A. Mooradian, Series in Material Science Vol. 18 (Springer-Verlag, Berlin, 1987), Chap. 3.

[2] G. Vitali, L. Palumbo, M. Rossi, G. Zollo, C. Pizzuto, L. Di Gaspare, and F. Evangelisti, Phys. Rev. B **53**, 4757 (1996).

[3] F. Jona, P. M. Marcus, H. L. Davis, and J. R. Noonan, Phys. Rev. B **33**, 4005 (1986).

[4] D. M. Zehner, C. W. White, and G. W. Ownby, Appl. Phys. Lett. **37**, 456 (1980).

[5] D. M. Zehner, C. W. White, P. Heimann, B. Reihl, F. J. Himpsel, and D. E. Eastman, Phys. Rev. B **24**, 4875 (1981).

[6] R. S. Becker, J. A. Golovchenko, G. S. Higashi, and B. S. Swartzentruber, Phys. Rev. Lett. **57**, 1020 (1986).

[7] H. Oefner, I. Ulrych, V. Chab, F. P. Netzer, and J. A. D. Matthew, Surf. Sci. **327**, 233 (1995).

[8] Y. J. Chabal, J. E. Rowe, and D. A. Zwemer, Phys. Rev. Lett. **46**, 600 (1981).

[9] V. Cháb, I. Lukeš, M. Ondřejček, and P. Jiříček, Prog. Surf. Sci. **35**, 197 (1990).

[10] *Semiconductors and Semimetals,* edited by R. F. Wood, C. W. White, and R. T. Young (Academic Press, New York, 1984), Vol. 23, Chap. 7, p. 405.

[11] D. Cvetko, V. De Renzi, L. Floreano, A. Morgante, M. Peloi, F. Tommasini, V. Cháb, and K. C. Prince, Phys. Rev. B **51**, 17 957 (1995).

[12] A. N. Vasil'ev, S. Yu. Karpov, Yu. V. Koval'chuk, V. E. Myachin, Yu. V. Pogorel'skii, M. Yu. Silova, I. A. Sokolov, and G. A. Fokin, Zh. Eksp. Teor. Fiz. **96**, 1459 (1989) [Sov. Phys. JETP **69**, 827 (1989)].

[13] R. Černý, V. Cháb, and P. Přikryl, Comput. Mater. Sci. **8**, 228 (1997).

[14] R. Černý and P. Přikryl, in *Numerical Methods in Thermal Problems,* edited by R. W. Lewis and J. T. Cross (Pineridge Press, Swansea, UK, 1997), Vol. X, p. 275.

[15] M. Born and E. Wolf, *Principles of Optics,* 6th ed. (Pergamon Press, Oxford, 1991).

[16] O. Borusík, R. Černý, P. Přikryl, K. M. El-Kader, I. Ulrych, Z. Chvoj, and V. Cháb, Appl. Surf. Sci. **109/110**, 317 (1997).

[17] E. Gatskevich, G. Ivlev, and A. Chaplanov, Quantum Electron. **25**, 805 (1995).

[18] R. Černý and P. Přikryl, Phys. Rev. B **57**, 194 (1998).